Available online at www.sciencedirect.com
ScienceDirect
Applied Surface Science 253 (2006) 1404–1410
applied surface science
www.elsevier.com/locate/apsusc

Effect of temperature on the sliding wear behavior of laser surface alloyed Ni-base on Al–Mg–Si alloy

Yao-Chih Chuang [a,*], Shih-Chin Lee [a], Hsin-Chih Lin [b]

[a] Department of Materials Science and Engineering, National Cheng Kung University, Tainan, Taiwan
[b] Department of Materials Science and Engineering, National Taiwan University, Taipei, Taiwan

Received 2 December 2005; accepted 9 February 2006
Available online 4 April 2006

Abstract

The surface microstructures of 6061 Al–Mg–Si alloy coated with laser surface alloyed (LSA) Ni–Cr–B–Si powder and their sliding wear performance have been investigated. Experimental results show that there are three regions, as grayish region (G.R.), dark region (D.R.) and bright region (B.R.), in the pool. The Al_3Ni and Al_3Ni_2 compounds appear in the G.R. and D.R., respectively. The Al–Ni–Cr amorphous structure can be observed in the B.R. The hardness of the LSA specimens is much higher than the Al-matrix. Compared with the Al-matrix, the LSA specimens have excellent sliding wear performance. They have lower friction coefficient and wear rate. The critical temperature of sliding wear resistance of LSA specimen is higher than that of Al-matrix by about 50 °C. The stress relief during thermal treatment will slightly reduce the hardness and the wear resistance of LSA specimens, especially at testing temperature >200 °C.

Keywords: Laser surface alloying; High temperature sliding wear; Nickel–chromium–boron–silicon powders

1. Introduction

Aluminum alloys have been used extensively in many industries because of their excellent properties, such as high thermal conductivity, excellent workability and high specific strength. But some drawbacks, like low hardness, poor tribological properties and crevice corrosion resistance, still need to be improved. In the past decades, a considerable number of studies have been made on how to improve the surface properties of aluminum alloys, involving the electroplating, chemical plating, anodizing and thermal spraying [1–3]. Recently, laser surface alloying (LSA) has been successfully developed to improve the surface properties of various metals and alloys, such as the surface mechanical/chemical properties of wear [4–7], corrosion [8–9] and cavitation erosion resistance [9–11]. Zhang et al. [12] investigated the wear resistance of Al alloys with and without reinforcement of Al_2O_3 particulates. They found that the Al alloys with reinforcement of Al_2O_3 particles by the LSA technique had a higher critical temperature of seizure than those without reinforcement. The ''critical temperature'' was defined as the temperature in which a mild wear changed to a severe wear. Song et al. [13] studied the wear properties of 6061 Al alloy with 3 and 20 μm SiC reinforced particulates. Their investigation found that the reinforcement of SiC particulates could effectively improve the wear resistance of 6061 Al alloy. Martínez et al. [14] worked on the sliding wear of Al–Si alloys and Al–Si/SiC composites at elevated temperatures, and demonstrated that the presence of hard SiC particulates increased the critical temperature by about 40 °C.

The Ni–Cr–B–Si powder is commercially available and is often used on the surface treatment of metals and alloys because of its low melting temperature and high hardness. This powder has been successfully laser-clad or laser surface alloyed onto steels [15], titanium alloys [16] and aluminum alloys [17]. One may notice that the Ni element in this powder has the same crystal lattice with Al, and hence the intermetallic compounds of Al_3Ni, Al_3Ni_2, AlNi and Ni_3Al are easily formed during the processes of laser cladding or laser surface alloying [18]. However, there is no systematic investigation of the LSA Ni–Cr–B–Si on the Al–Mg–Si alloys and their high temperature wear behavior. More experiments are necessary to be carried out to clarify the LSA characteristics on these aluminum alloys. Therefore, this paper aims to investigate the

* Corresponding author. Tel.: +886 6 275 7575x61506; fax: +886 6 238 4946.
E-mail address: MAXWELL@cubic.mse.ncku.edu.tw (Y.-C. Chuang).

0169-4332/$ – see front matter © 2006 Elsevier B.V. All rights reserved.
doi:10.1016/j.apsusc.2006.02.014

surface microstructures of 6061 Al–Mg–Si alloys coated with LSA Ni–Cr–B–Si. Their sliding wear performance is also discussed in this study.

2. Experimental procedure

The substrate material was an Al–Mg–Si alloy (ASTM 6061) with compositions of 1.0%Mg, 0.6%Si, 0.7%Fe, 0.27%Cu, 0.15%Zn, 0.15%Ti and the balance Al (in wt.%). The wear samples ($\Phi 35 \times 20$ mm^3) were machined from the as-extruded billets. Before LSA, the samples were sand blasted to increase the surface roughness and reduce the reflectivity of the laser beam. The chemical compositions of the Ni–Cr–B–Si powder are shown in Table 1. The Ni–Cr–B–Si powders are spherical particles with diameters of 70–200 μm. LSA was conducted with a 5 kW continuous transverse flow CO_2 laser. The diameter of laser beam was 2.5 mm with power density of 7.13×10^4 W/cm^2, and the laser scanning velocity was 10 mm/s. The sample surface was protected by argon gas during LSA. The powders were delivered to the pool with a flowing rate of about 2 g/min by a powder feeding system. In order to analyze the surface properties, the cross-sections of LSA samples were carefully cut perpendicular to the direction of laser scanning. Some LSA samples were subjected to a T6 treatment, namely, being solution-treated at 530 °C for 2 h, quenched in cold water, and then aged at 170 °C for 7 h, to compare their properties with the original LSA samples.

The surface microstructures were observed by using an Olympus BH2-UMA optical microscope (OM), a Hitachi S-4200 scanning electron microscope (SEM) and a Hitachi HF-2000 field emission transmission electron microscope (TEM). The compositions of surface layers were analyzed by using EDS attached to the SEM and TEM. A combined mechanical grinding and ion-beam thinning techniques was employed to prepare the TEM specimens. The hardness was measured by a Vickers Hardness Tester with a load of 50 g for 15 s. For each specimen, the average hardness value was calculated from at least five test readings.

The sliding wear behavior was examined by a ring-on-flat wear tester, as illustrated in Fig. 1. The testing temperature was precisely controlled between 25 and 250 °C. The flat was made of LSA sample and the counter-body disc was made of SKD61 with the following composition (wt.%): 0.39%C, 1.0%Si, 0.4%Mn, 5.2%Cr, 1.4%Mo, 0.8%V and the balance is Fe, which has a hardness of HV630. Before wear testing, the LSA sample was mechanized off about 0.3 mm from the surface and then polished to a roughness of Ra 0.13 μm in center-line-average. The operating parameters of sliding wear test were 19.6 N loading force, 0.7 m/s sliding speed and 1000 m sliding distance.

Table 1
The chemical compositions of the Ni–Cr–B–Si powder (in wt.%)

Element	Ni	Cr	B	Si	Fe	C
Ni–Cr–B–Si (wt.%)	Bal.	14.64	3.21	4.32	3.65	0.73

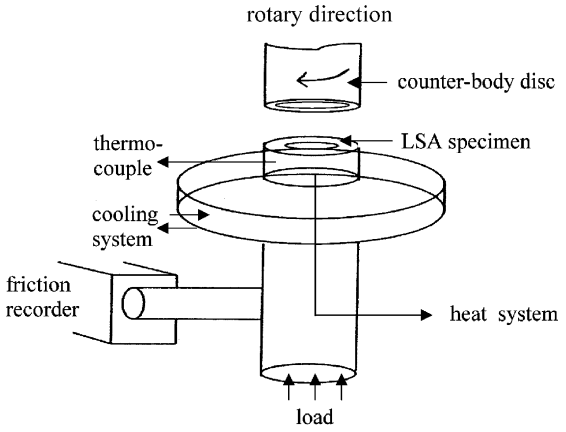

Fig. 1. A schematic representation of ring-on-flat type of wear equipment.

3. Results and discussion

3.1. Microstructure

Fig. 2 shows the photograph of the cross-section of the pool of LSA specimen. No cracks and porosity are observed in the melted pool. In Fig. 2, three distinct regions indicated as the grayish region (G.R.), dark region (D.R.) and bright region (B.R.) are clearly observed. The SEM observations of G.R. and D.R. are shown in Fig. 3(a and b), respectively. There shows a fine eutectic microstructure in the G.R. (Fig. 3(a)) and a needle-like microstructure in the D.R. (Fig. 3(b)). These fine eutectic and needle-like structures are identified to be Al_3Ni and Al_3Ni_2 compounds, respectively. Fig. 4(a and b) show the TEM micrograph and the diffraction analysis of the B.R. A typical halo pattern in Fig. 4(b) indicates that the B.R. has an amorphous structure. The chemical compositions of this amorphous structure are measured by EDS to be in the range of 44–47%Al, 42–43%Ni and 9–13%Cr (wt.%).

Fig. 5 shows the concentration profile of Al, Ni and Cr elements versus the depth from the surface to the bottom along the marked line in Fig. 2. In Fig. 5, one can see that Ni is dispersed all over the G.R., D.R. and B.R., but Cr only concentrates in the B.R., namely in the lower region of the

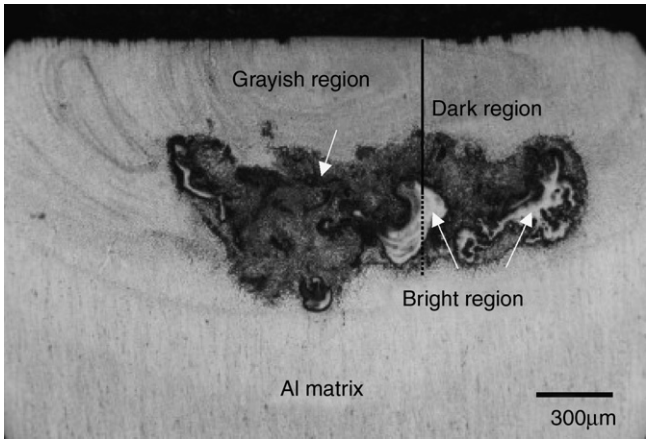

Fig. 2. Photograph of the transverse cross-section of the LSA specimen.

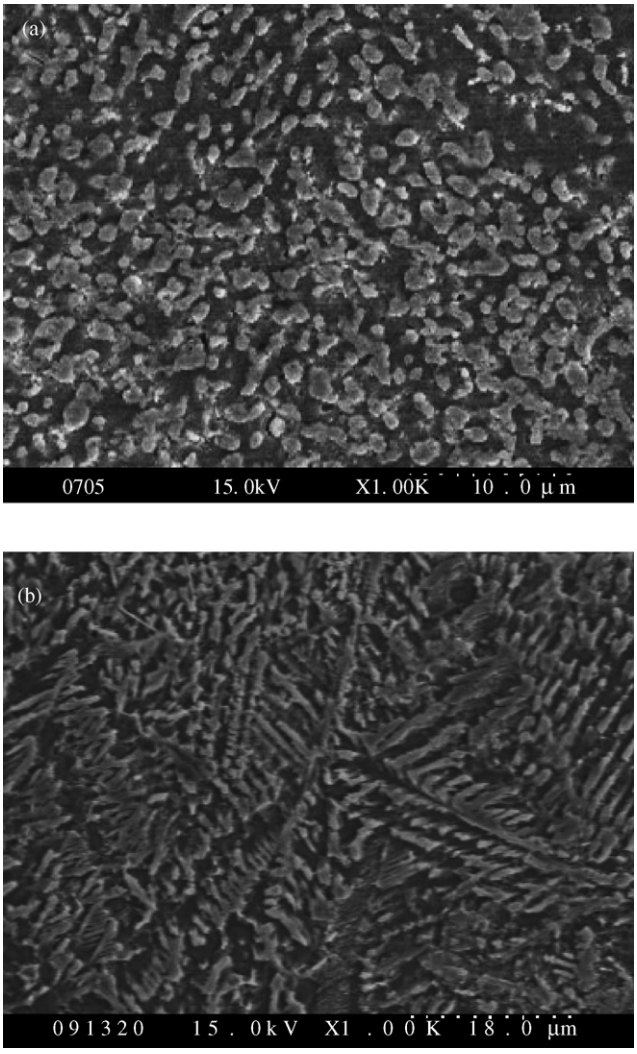

Fig. 3. SEM micrographs of the LSA specimen in the regions of (a) G.R. and (b) D.R.

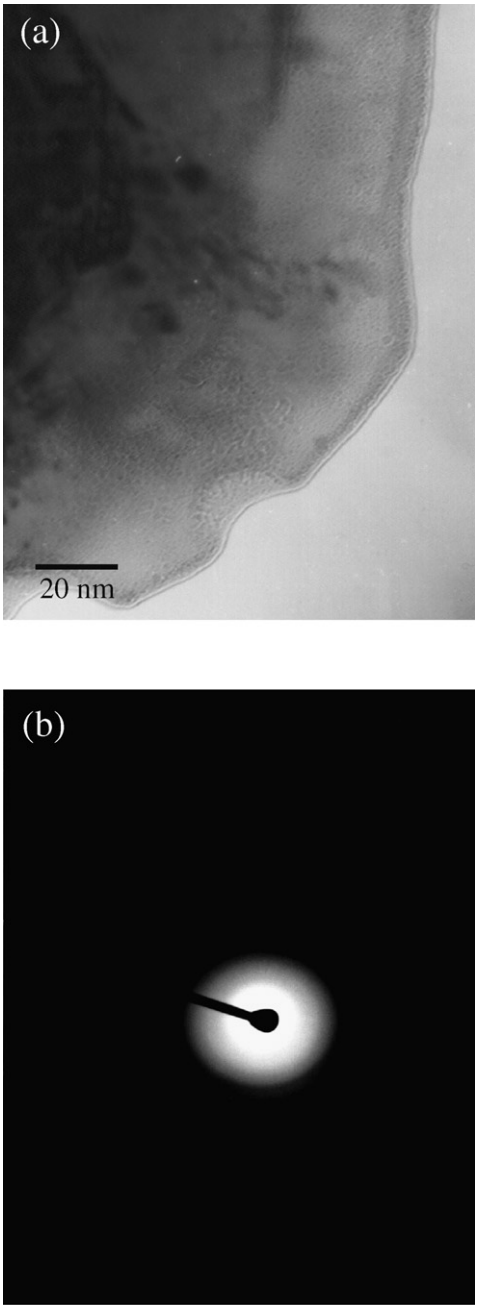

Fig. 4. TEM observation in the B.R. of the LSA specimen. (a) Bright field image; (b) diffraction pattern.

melted pool. This phenomenon can be ascribed to the lower diffusion coefficient and higher specific gravity of Cr than other elements. In Fig. 5, one can also find that the content of Ni increases obviously with increasing depth from the G.R. to D.R. This feature is ascribed to that the Ni element has a higher specific gravity than Al-matrix. The variation of Ni content is consistent with the formation of Al_3Ni in the G.R. and Al_3Ni_2 in the D.R. In the B.R., Ni content decreases slightly and Cr content increases as compared with that in other regions. It is well known that Cr can form solid solution with Ni in a large composition range [19], because that the atomic radius of Cr is very similar to Ni. As mentioned above, the Cr element mainly concentrates in the B.R. It is reasonable to postulate that the Cr atoms can replace some Ni atoms in Al–Ni compound to form Al–Ni–Cr compound. According to the ternary diagram of Al–Ni–Cr [20], the melting point of the B.R. is higher than 1300 °C. Besides, the average cooling rate is about 10^4 K/s [17,21] in the B.R. Hence, it is reasonable to form an amorphous structure in the B.R., as shown in Fig. 4.

3.2. Effects of heat treatment

To understand the effects of heat treatment, the LSA specimens were subjected to a T6 treatment, namely, being solution-treated at 530 °C for 2 h, quenched in cold water, and then aged at 170 °C for 7 h. After T6 treatment, the original Al_3Ni particles in the G.R. grew up and a lot of tiny Al_3Ni precipitates formed around the original Al_3Ni particles, as shown in Fig. 6(a). The similar phenomenon occurred for the needle-like Al_3Ni_2 particles. In Fig. 6(b), the original primary dendrites became blunt, and the dendrite arms almost disappeared after T6 treatment. It can also be observed that lots of tiny Al_3Ni precipitates were introduced within the

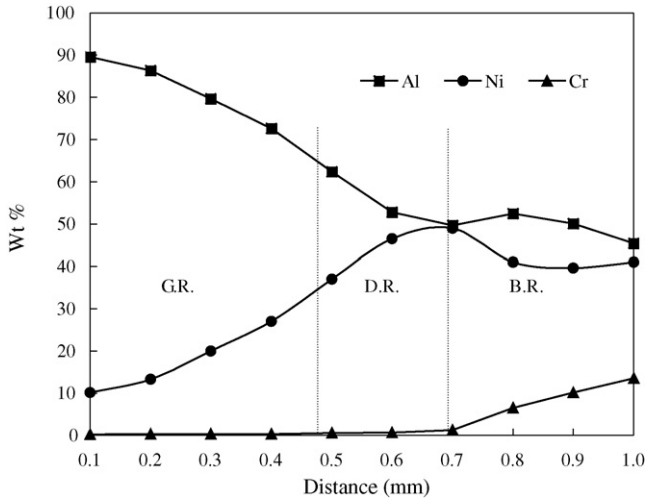

Fig. 5. The distribution of chemical compositions from surface to bottom of the pool.

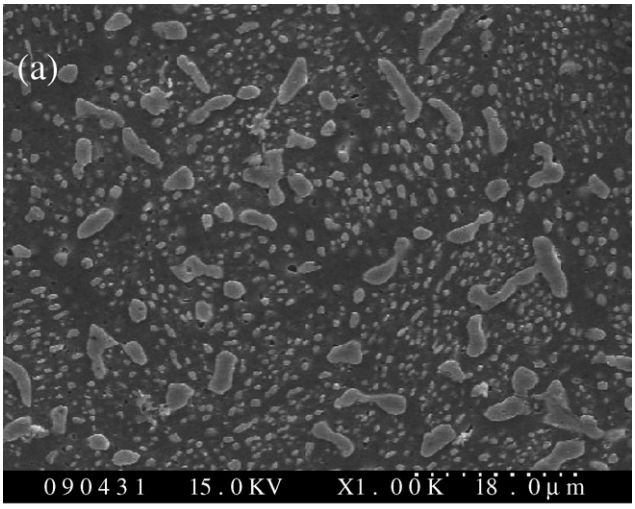

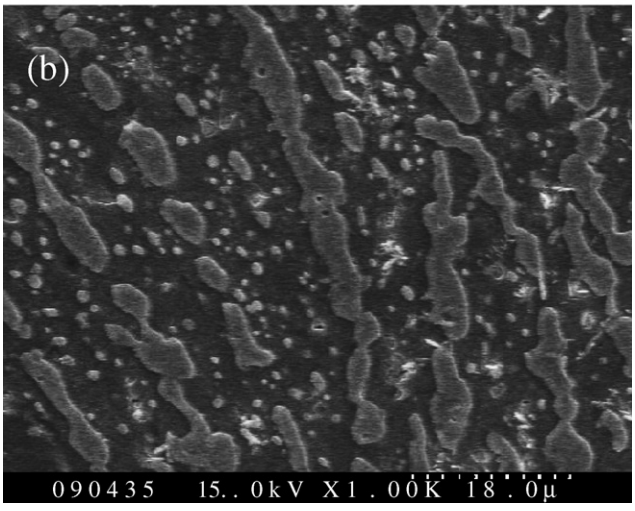

Fig. 6. SEM micrographs of the LSA specimen with T6 treatment. (a) G.R; (b) D.R.

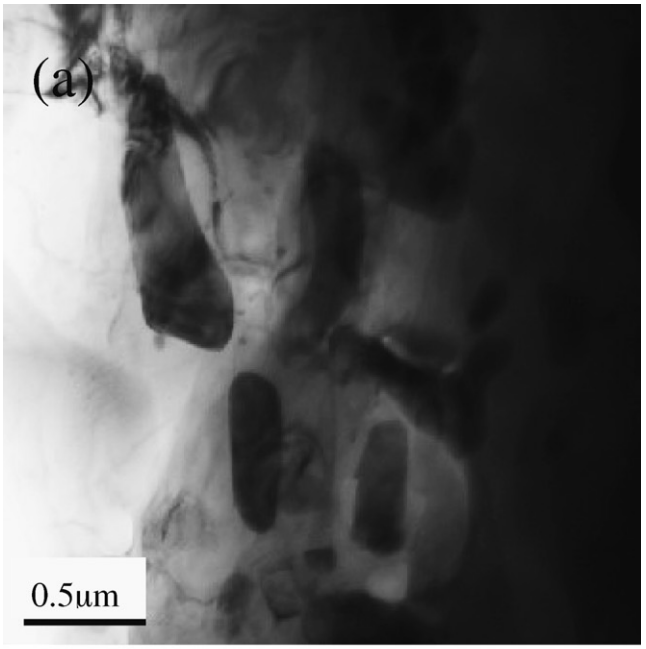

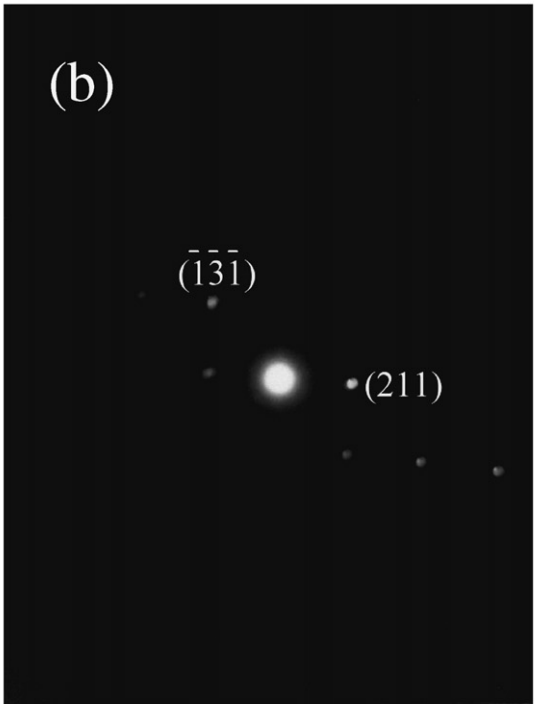

Fig. 7. TEM observation in the B.R. of the LSA specimen with T6 treatment. (a) Bright field image; (b) diffraction pattern.

matrix. Fig. 7(a and b) show the TEM micrograph and diffraction pattern of the B.R. for the LSA specimen with T6 treatment. According to the analysis of diffraction pattern in Fig. 7(b), the precipitates appear in Fig. 7(a) are identified to be Al_3Ni compounds. Therefore, it can simply conclude that the Al_3Ni compound can precipitate in G.R., D.R. and B.R. after T6 treatment. This result can be explained as follows. Because of the rapid solidification during the LSA process, there exists a large quantity of supersaturated Ni atoms. Hence, these excess

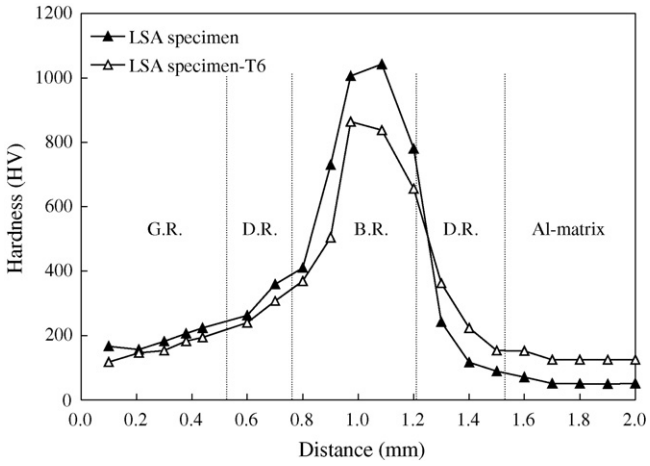

Fig. 8. The profiles of microhardness from the surface to Al-matrix of the LSA specimens.

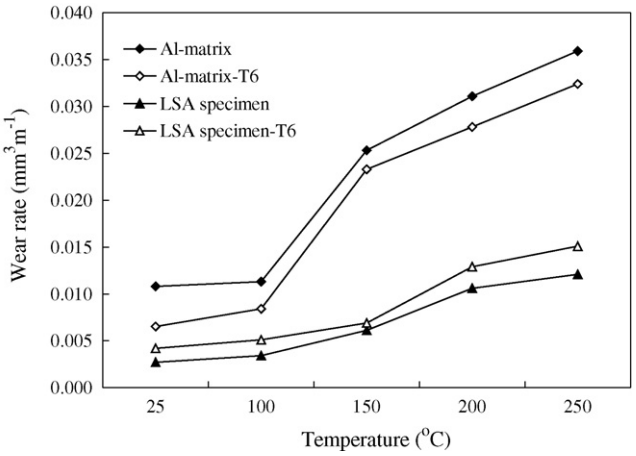

Fig. 9. The curves of wear rate vs. temperature for the specimens of Al-matrix, LSA specimens and T6 treated specimens.

Ni atoms will react with the Al atoms to form the Al_3Ni precipitates in the following T6 treatment.

3.3. Microhardness

Fig. 8 shows the profile of hardness versus depth from the surface to the Al-matrix along the marked line in Fig. 2 for the LSA specimen. It can be well realized that the G.R. and D.R. of the LSA specimen have higher hardness than the Al-matrix, due to the existence of Al_3Ni and Al_3Ni_2 compounds. In these regions of LSA specimen, the hardness can reach HV 125–400, which is approximately two to seven times of the Al-matrix (HV 60). The highest hardness for the LSA specimen is about HV 1100 and occurs in the B.R. The irregular arrangement of atoms of the amorphous structure in this region will introduce large internal stress and increase the hardness. Meanwhile, the large quantity of Cr atoms in this region will also raise its hardness. In Fig. 8, one can find that the hardness in the B.R. decreases a lot after T6 treatment. This feature is ascribed to the stress relief of the amorphous structure in this region.

3.4. Wear test

Wear tests were carried out at 25, 100, 150, 200 and 250 °C for both Al-matrix and LSA specimens. Figs. 9 and 10 show the wear rate and friction coefficient versus testing temperature of the wearing test, respectively. As shown in Fig. 9, the LSA specimens have very low wear rate, which is approximately four to eight times less than the Al-matrix at 25–250 °C. The wear rate of these specimens follows a relation: LSA specimen < LSA specimen (T6) < Al-matrix (T6) < Al-matrix. Since the LSA specimens have the Al_3Ni and Al_3Ni_2 reinforced particulates in the G.R. and D.R. and Al–Ni–Cr amorphous structure in the B.R., their hardness can increase to 2–18 times higher than that of Al-matrix, and thereby increase the wear resistance. It can also be observed in Fig. 9 that the slopes of wear rate versus testing temperature exhibit a significant increase between 100 and 150 °C for Al-matrix and between 150 and 200 °C for LSA specimens. The similar phenomenon is observed in Fig. 10 for the experimental data of friction coefficient versus testing temperature. These features indicate that the critical temperature of sliding wear resistance of LSA specimen is higher than that of Al-matrix by about 50 °C. This result is consistent with the viewpoint reported by Martinez et al. [14]. Fig. 11(a–c) show the SEM micrographs of the worn surface of LSA specimen which has been subjected to wear sliding at 100, 150 and 200 °C, respectively. As can be seen in Fig. 11(a), the worn surface is smooth and the ploughing strips are very shallow. This feature is ascribed to the fact that the Al_3Ni reinforced particles can improve the wear resistance in the mild sliding wear regime. Upon elevating the temperature to 150 °C, the surrounding Al-matrix begins to soften because its critical temperature of sliding wear resistance occurs between 100 and 150 °C (as seen in Fig. 9). This feature will reduce the reinforcement of Al_3Ni particles during the wear sliding. As seen in Fig. 11(b), the reinforced particles are removed from the edge of the strips and the worn surface exhibits a lot of wear debris. When the testing temperature

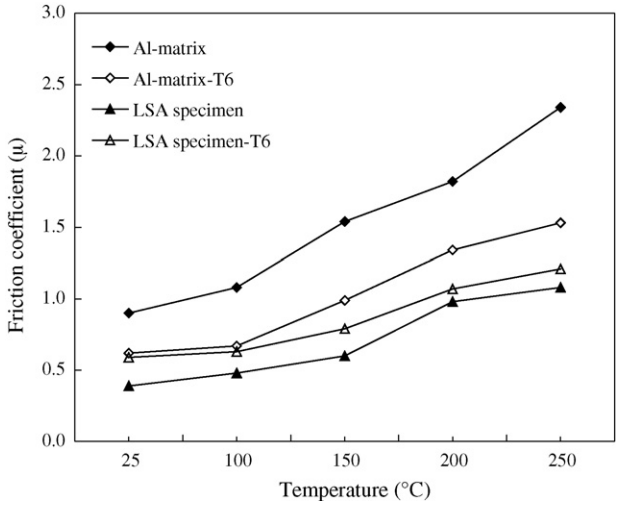

Fig. 10. The curves of friction coefficient vs. temperature for the specimens of Al-matrix, LSA specimens and T6 treated specimens.

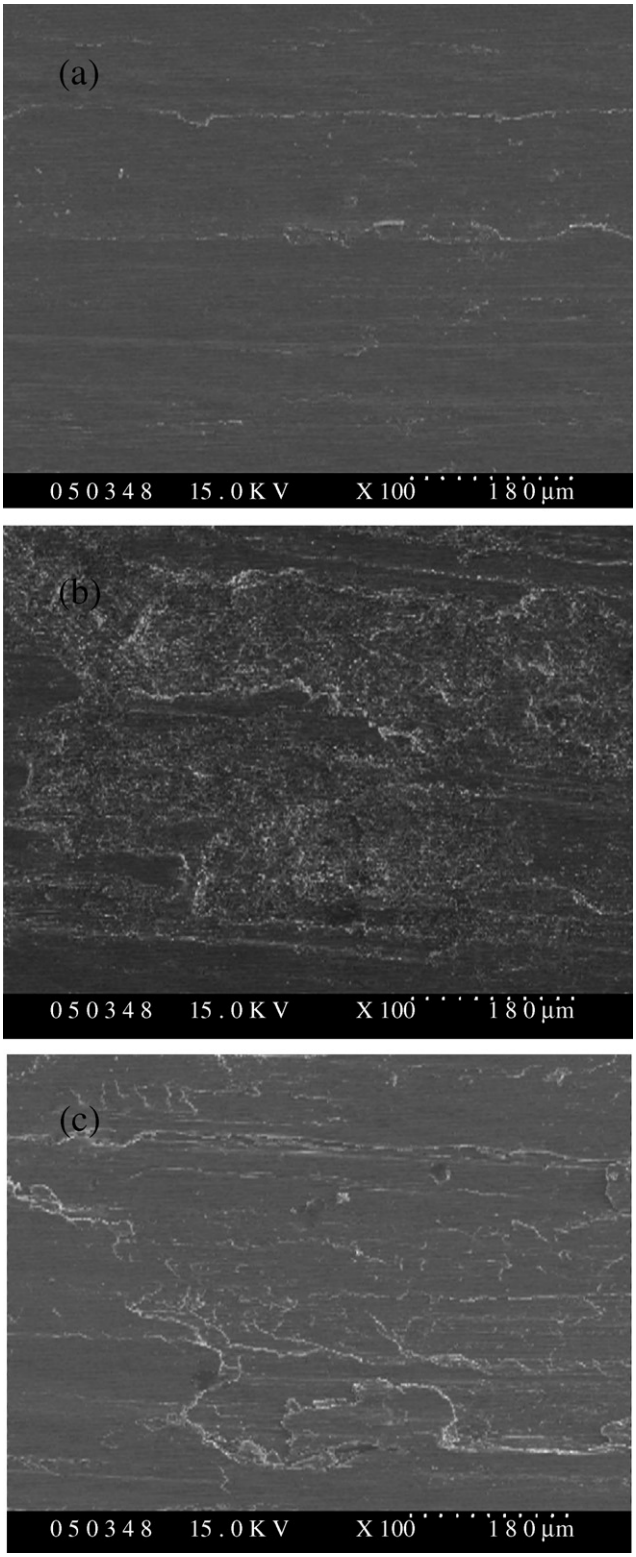

Fig. 11. SEM micrographs of the worn surfaces of LSA specimens with sliding wear at (a) 100 °C; (b) 150 °C; (c) 200 °C.

increases to 200 °C, the failure of Al_3Ni reinforced particles will result in the removal of the worn surface. However, the larger dimension and higher hardness of Al_3Ni_2 particles in the next region and Al–Ni–Cr amorphous structure in the B.R. will provide a more effective wear resistance even the temperature rises up to 200 °C, as shown in Fig. 11(c). This phenomenon can explain why the wear rate does not apparently increase from 200 to 250 °C in Fig. 9.

In Fig. 9, one can find that the T6 treatment has a little influence on the wear resistance of Al-matrix and LSA specimen. The wear rate of Al-matrix was slightly decreased by T6 treatment. It is because a large number of Mg_2Si has been precipitated in the Al-matrix by the peak-aged condition [13]. Therefore, the precipitates increased the hardness of the Al-matrix and thereby reduced the wear rate. On the other hand, the wear rate of LSA specimen was increased by T6 treatment, especially at testing temperature >200 °C. Apparently, the stress relief during the T6 treatment will slightly reduce the hardness and the wear resistance of LSA specimen.

4. Conclusions

The surface microstructures of 6061 Al–Mg–Si alloy coated with LSA Ni–Cr–B–Si powder and their sliding wear performance have been investigated. The important conclusions are as follows.

1. There are three distinct regions indicated as the grayish region, dark region and bright region in the melted zone of LSA specimen. The Al_3Ni and Al_3Ni_2 compounds appear in the grayish and dark regions, respectively. The Al–Ni–Cr amorphous structure can be observed in the bright region.
2. The LSA specimens have a much higher hardness than the Al-matrix. The hardness of Al–Ni–Cr amorphous structure in the bright region can even reach HV 1100, which is approximately 18 times of the Al-matrix.
3. The LSA specimens have a very low wear rate, which is approximately four to eight times less than that of the Al-matrix at 25–250 °C. Besides, the critical temperature of sliding wear resistance of LSA specimen is higher than that of Al-matrix by about 50 °C.
4. The stress relief in the laser-melted zone during T6 treatment will slightly reduce the hardness and the wear resistance of LSA specimens, especially at testing temperature >200 °C.

Acknowledgements

The authors are pleased to acknowledge the financial support of this research by the National Science Council (NSC), Republic of China, under grant no. NSC 89-2216-E-006-078.

Reference

[1] T. Suzuki, D. Huang, Y. Ikuhara, Surf. Coat. Technol. 107 (1998) 41–47.
[2] X.D. Peng, A. Kharlov, V. Bystritski, E. Garate, E.J. Lavernia, Mater. Sci. Eng. A 251 (1998) 142–149.
[3] K. Nakata, M. Ushio, Surf. Coat. Technol. 169–170 (2003) 443–446.
[4] L.J. Yang, Comp. Sci. Technol. 63 (2003) 575–583.
[5] Q. Ming, L.C. Lin, Z.D. Chen, Surf. Coat. Technol. 106 (1998) 174–182.
[6] Y.B. Liu, J.D. Hu, Z.Y. Cao, P.K. Rohatgi, Wear 206 (1997) 83–86.
[7] G.Y. Liang, T.T. Wong, J.M.K. MacAlpine, J.Y. Su, Surf. Coat. Technol. 127 (2000) 233–238.

[8] T.M. Yue, Y.X. Wu, H.C. Man, Surf. Coat. Technol. 114 (1999) 13–18.
[9] H.C. Man, S. Zhang, T.M. Yue, F.T. Cheng, Surf. Coat. Technol. 148 (2001) 136–142.
[10] W.J. Tomlinson, A.S. Bransden, Wear 185 (1995) 59–65.
[11] K.F. Tam, F.T. Cheng, H.C. Man, Surf. Coat. Technol. 149 (2002) 36–44.
[12] J. Zhang, A.T. Alpas, Mater. Sci. Eng. A 161 (1993) 273–284.
[13] W.Q. Song, P. Krauklis, A.P. Mouritz, S. Bandyopadhyay, Wear 185 (1995) 125–130.
[14] M.A. Martínez, A. Martín, J. Llorca, Metall. Mater. 28 (1993) 207–212.
[15] C.T. Kwok, F.T. Cheng, F.T. Cheng, H.C. Man, Surf. Coat. Technol. 107 (1998) 31–40.
[16] R.L. Sun, D.Z. Yang, L.X. Guo, S.L. Dong, Surf. Coat. Technol. 132 (2000) 251–255.
[17] G.Y. Liang, T.T. Wong, Surf. Coat. Technol. 89 (1997) 121–126.
[18] T.B. Massalski (Ed.), Binary Alloy Phase Diagrams, vol. 1, ASM Metal Park, 1986, p. 140.
[19] C.J. Smithells, Metal Reference Book, fifth ed., Butter-worth and Co. Ltd., London, 1976, p. 100.
[20] D.R.F. West, Ternary Equilibrium Diagrams, second ed., Chapman and Hall Ltd., New York, 1982, pp. 96–97.
[21] G.Y. Liang, C.L. Li, J.Y. Su, Mater. Sci. Eng. A 224 (1997) 173–176.